

Research Article

Dielectric properties of ammonium iron sulphate-dodecahydrate alum crystal

Muzaffar Iqbal Khan^{1*}, Riya Upadhyay², Rayees Ahmad Zargar¹, Majahid Ul Islam¹,
Feroz Ahmad Mir¹, Trilok Chandra Upadhyay²

¹Department of Physics, Baba Ghulam Shah Badshah University Rajouri (Jammu and Kashmir)-185234, India

²Department of Physics, Hemvati Nandan Bahuguna Garhwal University (A Central University) Srinagar (Garhwal), Uttarakhand-246174, India

E-mail: muzaffariqbalkhan786@gmail.com; Tel.: +919-536-122-318

Received: 6 August 2022; **Revised:** 24 October 2022; **Accepted:** 26 October 2022

Abstract: The statistical Green function theory and extended two sublattice pseudospin coupled-mode model Hamiltonian. The modified model summing with phonon anharmonic couplings, extra spin-lattice couplings and direct spin-spin coupling together with an applied electric field used to explain the dielectric properties of ammonium iron alum crystal (AFeSD-alum). The expressions for energy shift, linewidth, ferroelectric soft mode frequency, dielectric permittivity, and dielectric loss tangent are derived. By fitted the model values of different parameters in the above theoretical expressions. The thermal dependence of soft mode frequency, dielectric permittivity, and dielectric loss properties have been numerically calculated. Our theoretical obtained results compared well in agreement with experimental results reported by others.

Keywords: Green function; phonon anharmonic interactions; dielectric loss

1. Introduction

The behaviour of ammonium iron sulphate dodecahydrate ($\text{NH}_4\text{Fe}(\text{SO}_4)_2 \cdot 12\text{H}_2\text{O}$, abbreviated as AFeSD-alum) is typical of ferroelectric compounds [1]. AFeSD-alum correlated with the rotational motion of NH_4^{1+} -type of monovalent ions, each containing a rotational group. From the studies of neutron diffraction, it is concluded that a well-known asymmetric distribution of the hydrogen bonds in neighbouring the sulphate groups causes the ferroelectric phase transition in alums. But due to recent nuclear magnetic resonance studies and small thermal X-ray, the instability originating due to the asymmetrical arrangement of the bonding forces provide a high thermal dependence anharmonic contribution depending on the monovalent ions [1]. The AFeSD-alum crystal belongs to the alum family of double salts associated with the general chemical formula $\text{M}^{1+} \text{M}^{3+} (\text{RO}_4)_2 \cdot 12\text{H}_2\text{O}$, where M^{1+} is a monovalent ion ($\text{M}^{1+} = \text{NH}_4$) and M^{3+} is a trivalent metal such as Fe and R is S or Se forms an isomorphous series. AFeSD-alum is ferroelectric (phase II) below 88 K (-185°C) and above 88 K it is paraelectric (phase I), having a cubic crystal structure [2]. This symmetry difference from the paraelectric phase with Pa3 space group to the ferroelectric phase with Pca21 space group appears with the onset of ferroelectricity.

In AFeSD-alum NH_4^+ group gives rise to the order-disorder type of mechanism in the proton subsystem associated among these classes. This is important for the polar phase transition mechanism in alum compounds. Due to the order-

Copyright ©2022 Muzaffar Iqbal Khan, et al.

DOI: <https://doi.org/10.37256/mp01010005>

This is an open-access article distributed under a CC BY license

(Creative Commons Attribution 4.0 International License)

<https://creativecommons.org/licenses/by/4.0/>

disorder character of the ammonium family in AFeSD-alum, the hydrogen bonds correlated with these classes undergo some kind of ordering. Thus, the two sublattice pseudospin model Hamiltonian have applied similar to the case of potassium dihydrogen phosphate (KDP) system, after suitable modification. The proton motion is correlated with the active ammonium ion. Unlike the case of the hydrogen-bonded polar group, very little or nearly zero isotope effect is observed on deuteration at Curie temperature (T_c), demonstrating that the hydrogen-bonds are not primarily involved in the polar phase transition mechanism of alum compounds containing a large number of hydrogen bonds. The pseudospin motion should be greatly damped with strong anharmonic phonon couplings. The dielectric permittivity in AFeSD-alum crystal obeys the Curie-Weiss law in various interval ranges of temperature with ranges with one value of the Curie-Weiss constant (C). The unit cell lattice parameter for AFeSD-alum is at 25 °C and at 22 °C on deuteration [2]. The unit cell contains four ($Z=4$) formulas in the paraelectric phase (I) [2]. The density in per unit volume cell, $\rho = 1.73 \times 10^3 \text{ Kg m}^{-3}$ and on deuteration its value, $\rho = 1.812 \times 10^3 \text{ Kg m}^{-3}$ [1]. The crystal growth structure in AFeSD-alum by evaporation or cooling methods from aqueous solution.

There has considerable interest in the experimental and theoretical study of AFeSD-alum crystal. Campbell and DeBenedetti [3] have studied the Mossbauer spectra of the paramagnetic hyperfine structure of a dilute ammonium iron alum crystal. Morup and Thrane [4] have obtained relaxation Mossbauer spectra of AFeSD -alum crystal in the thermal range of 85–250 K, with the 0–5 kG an applied magnetic field. Weber [5] studied the electrogyration effect in the non-polar phase of ferroelectric alums. Kopcewicz et. al [6] obtained the Mossbauer spectrum measurements of proton irradiation effects in hydrated iron (II), ammonium sulphate, and iron (III) ammonium alum crystals. Roberts and Sambles [7] have studied the spin relaxation phenomena in AFeSD-alum crystal using Mossbauer spectroscopy, which explained that anomalous variations in linewidth with temperature should not be directly correlated with the polar phase transformation at 88 K. Lou and Yu [8] studied the dimorphism in methylammonium aluminum alum by X-ray diffraction and electron paramagnetic resonance. Cha and Strauss [9] have obtained the local structure and tunnelling energy of ammonium aluminum alum crystal by hole burning. Lui et al. [10] have studied morphology and compositional preparation of Al_2O_3 powders by spray pyrolysis of ammonium alum crystal. Ilhan et al. [11] have investigated the leachate by electrocoagulation using aluminum and iron alum electrodes. Mbow et al. [12] experimentally investigated the adjuvant action of ammonium iron alum crystal. Gu et al. [13] have studied the low-temperature thermal electrolytic coloration and spectral properties of ammonium alum crystals under various voltages. Yauri and Aliyu [14] studied the synthesis and analysis of potassium aluminium alum from a waste aluminium can. Gu and Li [15] studied the electrolytic coloration below 373 K and spectral properties of potassium alum crystals. Gu and Hao [16] studied the electrolytic coloration below 273 K and spectral representation properties of ammonium alum crystals with the help of a pointed anode. Petrushevski [17] studied the vibrational spectra and crystallographic results in a number of alums. Abdeen et al. [18] studied the X-ray and neutron diffraction in ferroelectric alum compounds. Chaudhury et al. [19] have proposed the anomalous dielectric behaviour in AFeSD-alum crystal with pseudospin lattice coupled-mode model Hamiltonian and statistical Green function theory. Rawat et al. [20] have obtained thermal variations of phase transition properties in AFeSD-alum crystal. Mamgain and Upadhyay [21] studied the thermal ferroelectric properties in AFeSD-alum crystal. Chaudhary et al. [19] have not studied third-order phonon anharmonic interactions. Moreover, they initially decoupled the correlation functions using the simple Tyablikov decoupling scheme. Earlier authors [19–21] have not considered indirect couplings, direct coupling, and an applied electric field in their study. Moreover, they have also decoupled the correlation functions at an early stage by using the simple decoupling scheme. As a result of some essential interactions were omitted from their numerical analysis. Ammonium iron sulphate-dodecahydrate, $(\text{NH}_4\text{Fe}(\text{SO}_4)_2 \cdot 12\text{H}_2\text{O})$, or $\text{NH}_4[\text{Fe}(\text{H}_2\text{O})_6](\text{SO}_4)_2 \cdot 6 \text{H}_2\text{O}$, also known as ferric ammonium sulphate or iron alum, is a double salt in the class of alums, which consists of compounds with the general formula $\text{M}^1 + \text{M}^3 + (\text{RO}_4)_2 \cdot 12\text{H}_2\text{O}$. It has the appearance of weakly violet, octahedral crystals. Ferric ammonium sulphate can be prepared by crystallization from a solution of ferric sulphate and ammonium sulphate. Iron in ferrous sulphate is oxidized to ferric sulphate by addition of sulfuric and nitric acid. Upon addition of ammonium sulphate to the solution and damping in of the solution, ferric ammonium sulphate crystals precipitate. Figure 1 shows the chemical structure depiction for ammonium iron sulphate-dodecahydrate alum crystal [22–24]. Equations for these conversions ignore the degree of hydration of the material. Oxidation equation: $6\text{FeSO}_4 + 2\text{HNO}_3 + 3\text{H}_2\text{SO}_4 = 3\text{Fe}_2(\text{SO}_4)_3 + 2\text{NO} + 4\text{H}_2\text{O}$ Synthesis equation: $\text{Fe}_2(\text{SO}_4)_3 + (\text{NH}_4)_2\text{SO}_4 = 2\text{NH}_4\text{Fe}(\text{SO}_4)_2$. Ammonium iron sulphate dodecahydrate is a reagent that is used as a mordant in dyeing and textile printing. It is also utilized in analytical chemistry as an iron standard. In biochemistry, ammonium ferric sulphate is used as a catalyst for the generation of free radicals. Increased xanthine oxidase and xanthine

oxidoreductase activity in cultured rat cells has been demonstrated in the presence of ammonium ferric sulphate. It may be used as an iron source to restore enzymatic activity in apoenzymes, such as for soybean lipoxygenase. It has been used in a wide range of various applications, from nanomaterials to general redox processes, and is frequently used as an analytical reference. Following are the major areas for use of ammonium iron sulphate dodecahydrate or ferric ammonium sulphate or iron alum crystal includes waste water treatment, tanning, production of dyestuffs, and as an etching agent in the production of electronic components. It has been used in a wide area of applications, including adiabatic refrigeration equipment, biochemical analysis and organic synthesis.

In this work, we have modified the two sublattice pseudospin lattice coupled-mode model Hamiltonian [19]. The model is modified by adding the anharmonic phonon couplings, the indirect coupling, the direct coupling and an applied electric field. With the help of retarded thermal Green function approach [25] and Dyson equation treatment, the theoretical expressions for energy shift, linewidth, ferroelectric soft mode frequency, dielectric permittivity, and dielectric loss tangent are derived. The numerical analysis of calculations will be done to obtain the temperature dependence of soft mode frequency, dielectric permittivity, and dielectric loss tangent properties by fitting the model parameter values. Theoretically obtained results will be compared in good agreement with experimental data reported by others [26].

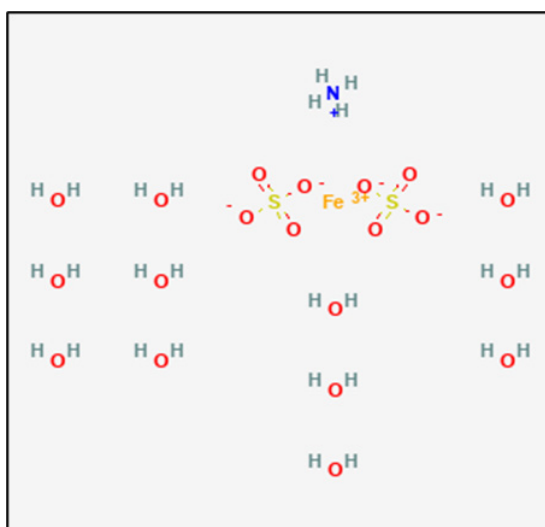


Figure 1. Chemical structure depiction for AFeSD crystal [22].

2. Model Hamiltonian for AFeSD-alum

The modified model Hamiltonian [19] for the coupled proton-phonon system summing the anharmonic phonon interactions, the indirect spin-lattice couplings, and the direct spin-spin coupling together with an applied electric field have used to explain the dielectric properties in AFeSD-alum crystal. The model Hamiltonian for the proton system in a rigid lattice is expressed.

$$\begin{aligned}
 H_1 = & -2\Omega \sum_i (S_{1i}^x + S_{2i}^x) - \sum_{ij} [J_{ij} (S_{1i}^z S_{1j}^z + S_{2i}^z S_{2j}^z) + K_{ij} S_{1i}^z S_{2j}^z] \\
 & - \sum_{ik} V_{ik} (S_{1i}^z A_k + S_{2i}^z A_k^\dagger) + \frac{1}{4} \sum_k w_k (A_k^\dagger A_k + B_k^\dagger B_k)
 \end{aligned} \quad (1)$$

where Ω represents the proton tunnelling energy, $S_\alpha^{x,z}$ called the component of pseudospin variable $\vec{S}_\alpha, \alpha = 1, 2$. Since we have considered the tunnelling integral value is small for AFeSD-alum to find its magnitude and make the

Hamiltonian comparable with that of the KDP-type problem. J_{ij} and K_{ij} are called the intrasublattice, and intersublattice coupling constants of the Ising-type, respectively, take the explanation of the long-range dipole-dipole forces. A_k , B_k and ω_k are represents respectively, the normal position, conjugate momentum associated wave vector k , and harmonic phonon frequency associated in terms of wave vector k . The third term in the above equation (1) describes the pseudospin interaction with polar optic phonons, causes the two potential wells for proton motion correlated with the methyl group to be nonequivalent. The model Hamiltonian in terms of anharmonic interactions, pseudospin phonon interactions can be expressed.

$$H_2 = \sum_{k_1 k_2 k_3} V^{(3)}(k_1, k_2, k_3) A_{k_1} A_{k_2} A_{k_3} - \sum_{k_1 k_2 k_3 k_4} V^{(4)}(k_1, k_2, k_3, k_4) A_{k_1} A_{k_2} A_{k_3} A_{k_4} - \sum_{ik} V_{ik} (S_{1i}^x A_k + S_{2i}^x A_k^\dagger) - \sum_{ik} V_{ik} (S_{1i}^x A_k^2 + S_{2i}^x A_k^{\dagger 2}) + \sum_{ij} B_{ij} (S_{1i}^x S_{1j}^x + S_{2i}^x S_{2j}^x) - 2\mu E \sum_i (S_{1i}^z + S_{2i}^z) \quad (2)$$

The first-term two terms of equation (2) represent the 3rd- and 4th-order phonon anharmonic [27] interactions part of the lattice vibrations. The third term explains the indirect spin-lattice coupling between the tunnelling motion of one proton to the tunnelling motion of another proton. The 4th term describes the interaction of the tunnelling motion with polar optic phonons. For the ferroelectric crystals that are not polar above the transition temperature, symmetry requires this interaction to be a square function of A. The polar-optic phonons make the two potential wells minima in the O-H-O bond unequivalent. The 5th term describes the direct spin-spin coupling between one proton's tunnelling motion and another's tunnelling motion in a transverse field Hamiltonian. The resultant Hamiltonian to explain the dielectric properties in AFeSD-alum crystal takes the form.

$$H = H_1 + H_2 \quad (3)$$

3. Green function theory for AFeSD-alum

Following Zubarev [25], we consider the thermal Green function $G(t - t')$ abbreviated as GF with two operators $S_{1i}^z(t)$ and $S_{1j}^z(t')$ be explained as (in units of $\hbar = 1$).

$$G(t - t') = \langle\langle S_{1i}^z(t); S_{1j}^z(t') \rangle\rangle = -i\theta(t - t') \langle [S_{1i}^z(t), S_{1j}^z(t')] \rangle \quad (4)$$

where theta (θ) represents the step unit function defined as $\theta = 1$ for $t > 0$; $\theta = 0$ for $t < 0$. $S_{1i}^z(t)$ and $S_{1j}^z(t')$ are the pseudospin variables in terms of z-components, $\langle \dots \rangle$ represents the statistical average over grand canonical ensemble for the enclosed operator, $[\dots]$ represents the notation for commutator and anticommutator operator and $\langle\langle \dots \rangle\rangle$ represents the notation for the corresponding Green function.

In the present work, we have studied the static properties and compared the theoretical results with other experimental data reported by others. Differentiating equation (4) with the help of model Hamiltonian, equation (3), then multiplying the equation on both sides by i we get.

$$i \frac{dG(t - t')}{dt} = \delta(t - t') \langle [S_{1i}^z(t), S_{1j}^z(t')] \rangle + \langle\langle [S_{1i}^z(t), H]; S_{1j}^z(t') \rangle\rangle \quad (5)$$

We have to take the differentiation of equation (5) again with respect to time t and multiply both sides by i , we get.

$$i^2 \frac{d^2 G(t - t')}{dt^2} = \delta(t - t') \langle\langle [S_{1i}^z(t), H], S_{1j}^z(t') \rangle\rangle + \langle\langle [S_{1i}^z(t), H]; [S_{1j}^z(t'), H] \rangle\rangle \quad (6)$$

With the help of the model Hamiltonian equation (3), and Dyson equation treatment and then taking the Fourier

transform we get.

$$G_{ij}(\omega) = \frac{2\Omega \langle S_{1i}^x \rangle \delta_{ij}}{(\omega^2 - 4\Omega^2)} + \frac{\langle \langle F_i(t); S_{1j}^z(t') \rangle \rangle}{(\omega^2 - 4\Omega^2)} \quad (7)$$

Now we have considered the Green function $\Gamma(t-t')$ defined as.

$$\Gamma(t-t') = \langle \langle F_i(t); S_{1j}^z(t') \rangle \rangle \quad (8)$$

Similarly, we have to differentiate equation (8) twice with respect to time t' and preceding similar to that of above, we get the Fourier transform of equation (7).

$$\Gamma(\omega) = \frac{\langle \langle F_i(t); F_j^\dagger(t') \rangle \rangle}{(\omega^2 - 4\Omega^2)} \quad (9)$$

where,

$$\begin{aligned} F_i(t) = & 2\Omega V_{ik} A_k S_{1i}^z + 2\Omega V_{ik} A_k^2 S_{1i}^z - 2\Omega J_{ij} (S_{1i}^x S_{1j}^z + S_{1i}^z S_{1j}^x \delta_{ij}) - 2\Omega V_{ik} A_k S_{1i}^x \\ & - V_{ik} A_k J_{ij} (S_{1i}^x S_{1j}^z + S_{1i}^z S_{1j}^x \delta_{ij}) - V_{ik} A_k^2 J_{ij} (S_{1i}^x S_{1j}^z + S_{1i}^z S_{1j}^x \delta_{ij}) \\ & - 2\Omega K_{ij} S_{1i}^x S_{2j}^z \delta_{ij} - V_{ik} A_k K_{ij} S_{1i}^x S_{2j}^z \delta_{ij} - V_{ik} A_k^2 K_{ij} S_{1i}^x S_{2j}^z \delta_{ij} - V_{ik}^2 A_k^2 S_{1i}^x \\ & + 2\Omega V_{ik} A_k S_{1i}^z + V_{ik}^2 A_k^2 S_{1i}^z + 2\Omega V_{ik} A_k^2 S_{1i}^z + 2\Omega B_{ij} (S_{1i}^x S_{1j}^z \delta_{ij} + S_{1i}^z S_{1j}^x) \\ & + V_{ik} A_k B_{ij} (S_{1i}^x S_{1j}^z \delta_{ij} + S_{1i}^z S_{1j}^x) + V_{ik} A_k^2 B_{ij} (S_{1i}^x S_{1j}^z \delta_{ij} + S_{1i}^z S_{1j}^x) - 4\Omega \mu E S_{1i}^x \\ & - 2\mu E V_{ik} A_k S_{1i}^x - 2\mu E V_{ik} A_k^2 S_{1i}^x \end{aligned} \quad (10)$$

And the F_j^\dagger is the complex conjugate of F_i .

$$\begin{aligned} F_j^\dagger(t') = & 2\Omega V_{ik} A_k^\dagger S_{1j}^z + 2\Omega V_{ik} A_k^{\dagger 2} S_{1j}^z - 2\Omega J_{ij} (S_{1i}^z S_{1j}^x + S_{1i}^x S_{1j}^z \delta_{ij}) \\ & - 2\Omega V_{ik} A_k^\dagger S_{1j}^x - V_{ik} A_k^\dagger J_{ij} (S_{1i}^z S_{1j}^x + S_{1i}^x S_{1j}^z \delta_{ij}) - V_{ik} A_k^{\dagger 2} J_{ij} (S_{1i}^z S_{1j}^x + S_{1i}^x S_{1j}^z \delta_{ij}) \\ & - 2\Omega K_{ij} S_{1i}^x S_{2j}^z \delta_{ij} - V_{ik} A_k^\dagger K_{ij} S_{1i}^x S_{2j}^z \delta_{ij} - V_{ik} A_k^{\dagger 2} K_{ij} S_{1i}^x S_{2j}^z \delta_{ij} - V_{ik}^2 A_k^{\dagger 2} S_{1i}^x \\ & + 2\Omega V_{ik} A_k^\dagger S_{1j}^z + V_{ik}^2 A_k^{\dagger 2} S_{1j}^z + 2\Omega V_{ik} A_k^{\dagger 2} S_{1j}^z + 2\Omega B_{ij} (S_{1i}^x S_{1j}^z + S_{1i}^z S_{1j}^x \delta_{ij}) \\ & + V_{ik} A_k^\dagger B_{ij} (S_{1i}^x S_{1j}^z + S_{1i}^z S_{1j}^x \delta_{ij}) + V_{ik} A_k^{\dagger 2} B_{ij} (S_{1i}^x S_{1j}^z + S_{1i}^z S_{1j}^x \delta_{ij}) - 4\Omega \mu E S_{1j}^x \\ & - 2\mu E V_{ik} A_k^\dagger S_{1j}^x - 2\mu E V_{ik} A_k^{\dagger 2} S_{1j}^x \end{aligned} \quad (11)$$

Substituting the value of $\Gamma(\omega)$ from equation (8) into equation (7) and then putting the resulting equation in the form Dyson equation form, we obtained.

$$G_{ij}(\omega) = G_{ij}^0(\omega) + G_{ij}^0(\omega) \tilde{R}(\omega) G_{ij}^0(\omega) \quad (12)$$

where,

$$G_{ij}^0 = \frac{\Omega \langle S_{1i}^x \rangle}{\pi \left[\omega^2 + \tilde{\Omega}^2 \right]} \quad (13)$$

$$\tilde{R}(\omega) = \frac{\pi \langle \langle F_i(t); F_i^\dagger(t') \rangle \rangle}{\Omega S_{ii}^x} \quad (14)$$

After simplifying the Dyson equation (12), we get the final expression of the thermal Green function equation (4).

$$G_{ij}(\omega) = \frac{\Omega S_{ii}^x \delta_{ij}}{\pi [\omega^2 - \tilde{\Omega}^2 - \tilde{R}(\omega)]} \quad (15)$$

And where the pseudospin frequency ($\tilde{\Omega}$) in equation (15) is expressed as.

$$\tilde{\Omega}^2 = a^2 + b^2 - bc \quad (16)$$

where,

$$a = 2J_{ij} \langle S_{ii}^z \rangle + K_{ij} \langle S_{ii}^z \rangle - 2B_{ij} \langle S_{ii}^z \rangle + 2\mu E \quad (17)$$

$$b = 2\Omega \quad (18)$$

$$c = 2J_{ij} \langle S_{ii}^x \rangle + K_{ij} \langle S_{ii}^x \rangle - 2B_{ij} \langle S_{ii}^x \rangle \quad (19)$$

The correlation functions of the higher-order Green functions in the Fourier transform of equation (9) are evaluated using the symmetric decoupling scheme to get the simpler Green functions and then put these values into the equation of response function in the Dyson equation. We obtained the response function with the help of a symmetric decoupling scheme done as follows: $\langle \langle PQ; RS \rangle \rangle = \langle PQ \rangle \langle \langle R; S \rangle \rangle + \langle PR \rangle \langle \langle Q; S \rangle \rangle + \langle PS \rangle \langle \langle Q; R \rangle \rangle + \langle QR \rangle \langle \langle P; S \rangle \rangle + \langle QS \rangle \langle \langle P; R \rangle \rangle + \langle RS \rangle \langle \langle P; Q \rangle \rangle$. We can get the response function, which is complex in nature, and break into the real and the imaginary parts known energy shift $\Delta(\omega)$ and line width $\Gamma(\omega)$, respectively.

4. Energy shift and line width for AFeSD-alum

For vanishing small quantity, the response function $\tilde{R}(\omega)$ can be resolved in terms of its complex form, i.e., the real and the imaginary parts, using the relation given.

$$\lim_{\varepsilon \rightarrow 0} \frac{1}{A \pm i\varepsilon} = \left(\frac{1}{A} \right)_P \pm i\pi\delta(A) \quad (20)$$

The real part called energy shift obtained as.

$$\begin{aligned}
 \Delta(\omega) = & \frac{a^4}{(\omega^2 - \tilde{\Omega}^2)} + \frac{b^2 c^2}{(\omega^2 - \tilde{\Omega}^2)} + \frac{16\Omega^2 V_{ik}^2 N_k}{(\omega^2 - \tilde{\Omega}^2)} + \frac{16\Omega V_{ik}^2 a \langle S_{1i}^z \rangle \omega_k (\omega^2 - \tilde{\omega}_k^2)}{\left((\omega^2 - \tilde{\omega}_k^2)^2 + 4\omega_k^2 \Gamma_k^2(\omega) \right) b} \\
 & + \frac{2\Omega V_{ik}^2 N_k a^2}{(\omega^2 - \tilde{\Omega}^2) b} + \frac{4\Omega V_{ik}^2 a \langle S_{1i}^x \rangle \omega_k (\omega^2 - \tilde{\omega}_k^2)}{\left((\omega^2 - \tilde{\omega}_k^2)^2 + 4\omega_k^2 \Gamma_k^2(\omega) \right)} + \frac{4V_{ik}^2 J_{ij}^2 N_k \langle S_{1i}^x \rangle^2}{(\omega^2 - \tilde{\Omega}^2)} + \frac{4V_{ik}^2 J_{ij}^2 N_k a^2 \langle S_{1i}^z \rangle^2}{(\omega^2 - \tilde{\Omega}^2) b^2} \\
 & + \frac{4V_{ik}^2 J_{ij}^2 \langle S_{1i}^x \rangle \langle S_{1j}^z \rangle^2 \omega_k (\omega^2 - \tilde{\omega}_k^2)}{\Omega \left((\omega^2 - \tilde{\omega}_k^2)^2 + 4\omega_k^2 \Gamma_k^2(\omega) \right)} + \frac{V_{ik}^2 K_{ij}^2 N_k \langle S_{1i}^x \rangle^2}{(\omega^2 - \tilde{\Omega}^2)} + \frac{V_{ik}^2 K_{ij}^2 N_k a^2 \langle S_{2j}^z \rangle^2}{(\omega^2 - \tilde{\Omega}^2) b^2} \\
 & + \frac{V_{ik}^2 K_{ij}^2 \langle S_{1i}^x \rangle \langle S_{2j}^z \rangle^2 \omega_k (\omega^2 - \tilde{\omega}_k^2)}{\Omega \left((\omega^2 - \tilde{\omega}_k^2)^2 + 4\omega_k^2 \Gamma_k^2(\omega) \right)} + \frac{4V_{ik}^2 N_k \langle S_{1i}^x \rangle \omega_k (\omega^2 - \tilde{\omega}_k^2)}{\Omega \left((\omega^2 - \tilde{\omega}_k^2)^2 + 4\omega_k^2 \Gamma_k^2(\omega) \right)} + \frac{2\Omega V_{ik}^2 N_k \langle S_{1j}^x \rangle}{(\omega^2 - \tilde{\Omega}^2)} \\
 & + \frac{4V_{ik}^2 B_{ij}^2 N_k \langle S_{1i}^x \rangle^2}{(\omega^2 - \tilde{\Omega}^2)} + \frac{4V_{ik}^2 B_{ij}^2 \langle S_{1j}^z \rangle^2 \omega_k (\omega^2 - \tilde{\omega}_k^2)}{\Omega \left((\omega^2 - \tilde{\omega}_k^2)^2 + 4\omega_k^2 \Gamma_k^2(\omega) \right)} + \frac{4\mu^2 E^2 V_{ik}^2 N_k a^2}{(\omega^2 - \tilde{\Omega}^2) b^2} \\
 & + \frac{4\mu^2 E^2 V_{ik}^2 \langle S_{1j}^x \rangle \omega_k (\omega^2 - \tilde{\omega}_k^2)}{\Omega \left((\omega^2 - \tilde{\omega}_k^2)^2 + 4\omega_k^2 \Gamma_k^2(\omega) \right)}
 \end{aligned} \tag{21}$$

The imaginary part called the line width obtained as.

$$\begin{aligned}
\Gamma(\omega) = & \frac{a^4}{2\tilde{\Omega}} [\tilde{\delta}(\omega - \tilde{\Omega}) - \tilde{\delta}(\omega + \tilde{\Omega})] + \frac{b^2 c^2}{2\tilde{\Omega}} [\tilde{\delta}(\omega - \tilde{\Omega}) - \tilde{\delta}(\omega + \tilde{\Omega})] \\
& + \frac{16\Omega^2 V_{ik}^2 N_k}{2\tilde{\Omega}} [\tilde{\delta}(\omega - \tilde{\Omega}) - \tilde{\delta}(\omega + \tilde{\Omega})] + \frac{32\Omega V_{ik}^2 a \langle S_{li}^z \rangle \omega_k^2 \Gamma_k(\omega)}{\left[(\omega^2 - \tilde{\omega}_k^2)^2 + 4\omega_k^2 \Gamma_k^2(\omega) \right] b} \\
& + \frac{2\Omega V_{ik}^2 N_k a^2}{2\tilde{\Omega} b} [\tilde{\delta}(\omega - \tilde{\Omega}) - \tilde{\delta}(\omega + \tilde{\Omega})] + \frac{8V_{ik}^2 \Omega \langle S_{li}^x \rangle \omega_k^2 \Gamma_k(\omega)}{\left[(\omega^2 - \tilde{\omega}_k^2)^2 + 4\omega_k^2 \Gamma_k^2(\omega) \right]} \\
& + \frac{4V_{ik}^2 N_k J_{ij}^2 \langle S_{li}^x \rangle^2}{2\tilde{\Omega}} [\tilde{\delta}(\omega - \tilde{\Omega}) - \tilde{\delta}(\omega + \tilde{\Omega})] + \frac{4V_{ik}^2 J_{ij}^2 N_k a^2 \langle S_{li}^x \rangle^2}{2\tilde{\Omega} b^2} \\
& \quad \left[\tilde{\delta}(\omega - \tilde{\Omega}) - \tilde{\delta}(\omega + \tilde{\Omega}) \right] + \frac{8V_{ik}^2 J_{ij}^2 \langle S_{li}^x \rangle \langle S_{lj}^z \rangle^2 \omega_k^2 \Gamma_k(\omega)}{\Omega \left[(\omega^2 - \tilde{\omega}_k^2)^2 + 4\omega_k^2 \Gamma_k^2(\omega) \right]} \\
& + \frac{V_{ik}^2 K_{ij}^2 N_k \langle S_{li}^x \rangle^2}{2\tilde{\Omega}} [\tilde{\delta}(\omega - \tilde{\Omega}) - \tilde{\delta}(\omega + \tilde{\Omega})] + \frac{V_{ik}^2 K_{ij}^2 N_k a^2 \langle S_{2j}^z \rangle^2}{2\tilde{\Omega} b^2} \\
& \quad \left[\tilde{\delta}(\omega - \tilde{\Omega}) - \tilde{\delta}(\omega + \tilde{\Omega}) \right] + \frac{2V_{ik}^2 K_{ij}^2 \langle S_{li}^x \rangle \langle S_{2j}^z \rangle^2 \omega_k^2 \Gamma_k(\omega)}{\Omega \left[(\omega^2 - \tilde{\omega}_k^2)^2 + 4\omega_k^2 \Gamma_k^2(\omega) \right]} \\
& + \frac{16V_{ik}^2 N_k \langle S_{li}^x \rangle \omega_k^2 \Gamma_k(\omega)}{b \left[(\omega^2 - \tilde{\omega}_k^2)^2 + 4\omega_k^2 \Gamma_k^2(\omega) \right]} + \frac{2\Omega V_{ik}^2 N_k \langle S_{lj}^x \rangle}{2\tilde{\Omega}} [\tilde{\delta}(\omega - \tilde{\Omega}) - \tilde{\delta}(\omega + \tilde{\Omega})] \\
& + \frac{4V_{ik}^2 B_{ij}^2 N_k \langle S_{lj}^x \rangle^2}{2\tilde{\Omega}} [\tilde{\delta}(\omega - \tilde{\Omega}) - \tilde{\delta}(\omega + \tilde{\Omega})] + \frac{16V_{ik}^2 B_{ij}^2 \langle S_{lj}^z \rangle^2 \omega_k^2 \Gamma_k(\omega)}{b \left[(\omega^2 - \tilde{\omega}_k^2)^2 + 4\omega_k^2 \Gamma_k^2(\omega) \right]} \\
& + \frac{4\mu^2 E^2 V_{ik}^2 N_k a^2}{2\tilde{\Omega} b^2} [\tilde{\delta}(\omega - \tilde{\Omega}) - \tilde{\delta}(\omega + \tilde{\Omega})] + \frac{16\mu^2 E^2 V_{ik}^2 \langle S_{lj}^x \rangle \omega_k^2 \Gamma_k(\omega)}{b \left[(\omega^2 - \tilde{\omega}_k^2)^2 + 4\omega_k^2 \Gamma_k^2(\omega) \right]}
\end{aligned} \tag{22}$$

In the above equations (21) and (22), $\tilde{\omega}_k$ represents the renormalized phonon frequency and $\Gamma_k(\omega)$ is the phonon line width due to the contribution of phonon anharmonic interactions. We have evaluated the phonon Green function $\langle\langle P_k(t); P_k^\dagger(t') \rangle\rangle$, it is obtained as.

$$\langle\langle P_k(t); P_k^\dagger(t') \rangle\rangle = \frac{4\omega_k \delta_{kk'}}{4\pi \left[\omega^2 - \tilde{\omega}_k^2 - i2\omega_k \Gamma_k(\omega) \right]} \tag{23}$$

where, $\tilde{\omega}_k$ is known as renormalized phonon frequency obtained as.

$$\tilde{\omega}_k^2 = \tilde{\omega}_k^2 + 2\omega_k A_k(\omega) \tag{24}$$

We get the pseudospin phonon frequency ($\tilde{\omega}_k$) as.

$$\tilde{\omega}_k^2 = \omega_k^2 + A(k, T) \quad (25)$$

The phonon energy shift $\Delta_k(\omega)$ for phonon Green function $\langle\langle P_k(t); P_k^\dagger(t') \rangle\rangle$ in equation (23), obtained as.

$$\begin{aligned} \Delta_k(\omega) = & 18\pi \sum_{k_1, k_2} \left| V^{(3)}(k_1, k_2, -k) \right|^2 \left(\frac{\omega_{k_1} \omega_{k_2}}{\tilde{\omega}_{k_1} \tilde{\omega}_{k_2}} \right) \\ & \times \left\{ (\tilde{n}_{k_1} + \tilde{n}_{k_2}) \frac{\tilde{\omega}_{k_1} + \tilde{\omega}_{k_2}}{\omega^2 - (\tilde{\omega}_{k_1} + \tilde{\omega}_{k_2})^2} + (\tilde{n}_{k_2} - \tilde{n}_{k_1}) \frac{\tilde{\omega}_{k_1} - \tilde{\omega}_{k_2}}{\omega^2 - (\tilde{\omega}_{k_1} - \tilde{\omega}_{k_2})^2} \right\} \\ & + 48\pi \sum_{k_1, k_2, k_3} \left| V^{(4)}(k_1, k_2, k_3, -k) \right|^2 \left(\frac{\omega_{k_1} \omega_{k_2} \omega_{k_3}}{\tilde{\omega}_{k_1} \tilde{\omega}_{k_2} \tilde{\omega}_{k_3}} \right) \\ & \times \left\{ (1 + \tilde{n}_{k_1} \tilde{n}_{k_2} + \tilde{n}_{k_2} \tilde{n}_{k_3} + \tilde{n}_{k_3} \tilde{n}_{k_1}) \frac{\tilde{\omega}_{k_1} + \tilde{\omega}_{k_2} + \tilde{\omega}_{k_3}}{\omega^2 - (\tilde{\omega}_{k_1} + \tilde{\omega}_{k_2} + \tilde{\omega}_{k_3})^2} \right. \\ & \left. + 3(1 - \tilde{n}_{k_1} \tilde{n}_{k_2} + \tilde{n}_{k_2} \tilde{n}_{k_3} - \tilde{n}_{k_3} \tilde{n}_{k_1}) \frac{\tilde{\omega}_{k_1} - \tilde{\omega}_{k_2} - \tilde{\omega}_{k_3}}{\omega^2 - (\tilde{\omega}_{k_1} - \tilde{\omega}_{k_2} - \tilde{\omega}_{k_3})^2} \right\} \\ & + \text{higher order terms} \end{aligned} \quad (26)$$

The phonon linewidth $\Gamma_k(\omega)$ for phonon Green function $\langle\langle P_k(t); P_k^\dagger(t') \rangle\rangle$ in equation (23), obtained as.

$$\begin{aligned} \Gamma_k(\omega) = & 18\pi \sum_{k_1, k_2} \left| V^{(3)}(k_1, k_2, -k) \right|^2 \left(\frac{\omega_{k_1} \omega_{k_2}}{\tilde{\omega}_{k_1} \tilde{\omega}_{k_2}} \right) \\ & \times [(\tilde{n}_{k_1} + \tilde{n}_{k_2}) \{ \delta(\omega + \tilde{\omega}_{k_1} + \tilde{\omega}_{k_2}) - \delta(\omega - \tilde{\omega}_{k_1} - \tilde{\omega}_{k_2}) \} \\ & + (\tilde{n}_{k_2} - \tilde{n}_{k_1}) \{ \delta(\omega - \tilde{\omega}_{k_1} - \tilde{\omega}_{k_2}) - \delta(\omega - \tilde{\omega}_{k_1} - \tilde{\omega}_{k_2} + \tilde{\omega}_{k_3}) \}] \\ & + 48\pi \sum_{k_1, k_2, k_3} \left| V^{(4)}(k_1, k_2, k_3, -k) \right|^2 \left(\frac{\omega_{k_1} \omega_{k_2} \omega_{k_3}}{\tilde{\omega}_{k_1} \tilde{\omega}_{k_2} \tilde{\omega}_{k_3}} \right) \\ & \times [(1 + \tilde{n}_{k_1} \tilde{n}_{k_2} + \tilde{n}_{k_2} \tilde{n}_{k_3} + \tilde{n}_{k_3} \tilde{n}_{k_1}) \{ \delta(\omega + \tilde{\omega}_{k_1} - \tilde{\omega}_{k_2}) - \delta(\omega - \tilde{\omega}_{k_1} - \tilde{\omega}_{k_2} + \tilde{\omega}_{k_3}) \} \\ & + 3(1 - \tilde{n}_{k_1} \tilde{n}_{k_2} + \tilde{n}_{k_2} \tilde{n}_{k_3} - \tilde{n}_{k_3} \tilde{n}_{k_1}) \{ \delta(\omega + \tilde{\omega}_{k_1} - \tilde{\omega}_{k_2}) - \delta(\omega - \tilde{\omega}_{k_1} - \tilde{\omega}_{k_2} + \tilde{\omega}_{k_3}) \}] \\ & + \text{higher order terms} \end{aligned} \quad (27)$$

and

$$\tilde{n}_k = \frac{\omega_k}{\tilde{\omega}_k} \tanh\left(\frac{4\pi k_B T}{h\tilde{\omega}_k}\right) \quad (28)$$

where, k_B called the Boltzmann constant; T represents the absolute temperature.

5. Soft mode frequency for AFeSD-alum

The response function $\tilde{R}(\omega)$ in terms of complex nature and evaluated with the help of a symmetric decoupling scheme and provides the final expression of the retarded Green function equation (15) obtained as

$$G_{ij}(\omega + i\varepsilon) = \frac{\langle S_{ij}^x \rangle \Omega \delta_{ij}}{\pi \left[\omega^2 - \hat{\Omega}^2 - 2i\Omega\Gamma(\omega) \right]} \quad (29)$$

where the soft mode frequency $(\hat{\Omega})$ is expressed by.

$$\hat{\Omega}^2 = \tilde{\Omega}^2 + 2\Omega\Delta(\omega) \quad (30)$$

and the modified pseudospin frequency $(\tilde{\Omega})$ is expressed as.

$$\tilde{\Omega}^2 = \bar{\Omega}^2 + 2\Delta(\omega) \quad (31)$$

where $\bar{\Omega}$ in equation (30) represents the renormalized pseudospin frequency. According to Cochran's novel idea [28] for ferroelectricity that the ferroelectric crystals should be stable for small deformations, that a soft optic mode of atomic lattice vibrations have real frequencies, and the corresponding frequency goes to a minimum (soften) at a Curie temperature reached. This is known as ferroelectric soft mode frequency. Solving the ferroelectric soft mode frequency equation (30) persistently, we obtained the final expression for soft mode frequency $(\hat{\Omega})$, it is obtained as

$$\hat{\Omega}^2 = \left[\frac{\left(\omega_k^2 + \tilde{\Omega}^2 \right)}{2} \pm \frac{1}{2} \left\{ \left(\omega_k^2 + \tilde{\Omega}^2 \right)^2 + 4 \left\{ \frac{8V_{ik}^2 a S_{li}^z \omega_k + 4\Omega V_{ik}^2 S_{li}^x \omega_k + \frac{4V_{ik}^2 J_{ij}^2 S_{li}^x S_{li}^z \omega_k}{\Omega}}{\Omega} + \frac{V_{ik}^2 K_{ij}^2 S_{li}^x S_{2j}^z \omega_k}{\Omega} + \frac{4V_{ik}^2 N_k S_{li}^x \omega_k}{\Omega} + \frac{8V_{ik}^2 B_{ij}^2 S_{lj}^z \omega_k}{b} + \frac{8\mu^2 E^2 V_{ik}^2 N_k S_{lj}^x \omega_k}{b} \right\} \right\}^{\frac{1}{2}} \right] \quad (32)$$

The equation (32) represents the soft mode frequency $(\hat{\Omega})$ depends on the anharmonic phonon couplings, indirect spin-lattice coupling, and direct spin-spin coupling together with external electric field terms, which is nearly equal to zero (condensed) at phase transition temperature in the transverse optical lattice vibration mode responsible for the phase transition mechanism in AFeSD-alum crystal.

6. Dielectric constant and tangent loss for AFeSD-alum crystal

The dielectric susceptibility conveniently expresses the response function of ferroelectric crystals to an applied external electric field. Following the Zubarev [25] and Kubo [29] formalism, we obtained the complex dielectric susceptibility $\chi_{ij}(\omega)$ in a tensor form related to the retarded Green function $G_{ij}(\omega + i\varepsilon)$ obtained by the relation.

$$\chi_{ij}(\omega) = -\lim_{\varepsilon \rightarrow 0} 2\pi\mu^2 N G_{ij}(\omega + i\varepsilon) \quad (33)$$

where N represents the total sum of dipoles and mu (μ) denotes the dipole moment associated with O-H--O bond. The relative permittivity $\varepsilon(\omega)$ and dielectric susceptibility $\chi_{ij}(\omega)$ are formulated by the relation obtained as.

$$\varepsilon(\omega) = (1 + 4\pi\chi_{ij}) \quad (34)$$

For simplifying calculations of ferroelectric crystals, we assume $\varepsilon \gg 1$. Therefore, we neglect the one from equation (34). With the help of equations (33) and (34) and thermal Green function, we get the relative permittivity $\varepsilon(\omega)$ obtained as.

$$\varepsilon(\omega) = \frac{-8\pi N\Omega\mu^2 \langle S_{i_i}^x \rangle \left[(\omega^2 - \widehat{\Omega}^2) + 2i\Omega\Gamma(\omega) \right]}{\left[(\omega^2 - \widehat{\Omega}^2)^2 + 4\Omega^2\Gamma^2(\omega) \right]} \quad (35)$$

The equation (35) shows that the relative permittivity for AFeSD-alum crystal depends directly on tunnelling energy, the pseudospin variable in the x-component, and is inversely proportional to the square of the soft mode frequency and total width.

In ferroelectric AFeSD-alum crystal, some power losses developed in the form of electromagnetic energy that separates the losses due to conduction and those due to spontaneous polarization properties of dielectric materials. The useful method to explain the losses in the ferroelectric crystals is by means of the dielectric loss tangent obtained by the correlation of the imaginary to the real parts of the complex dielectric permittivity. It is represented by $\tan \delta$ and expressed as.

$$\tan \delta = \frac{\text{imaginary part of } \varepsilon(\omega)}{\text{real part of } \varepsilon(\omega)} = -\frac{2\Gamma(\omega)\Omega}{(\omega^2 - \widehat{\Omega}^2)} \quad (36)$$

From equation (36), we observe that the loss tangent depends directly on tunnelling energy and total width and is inversely proportional to the difference square of the harmonic phonon frequency and the square of the ferroelectric mode frequency.

7. Numerical calculations for AFeSD-alum crystal

For the study of dielectric properties of AFeSD-alum crystal. We have done modelling of the different physical quantities for AFeSD-alum compound, as shown in table 1 obtained by modelled and from the literature for numerical analysis.

Table 1. Model values of various physical parameters for AFeSD-alum [19]

Physical parameters	Parameter values	Unit in symbols
T_c	88	K
C	425	K
Ω	0.15	cm^{-1}
V_{ik}	6.49	cm^{-1}
J_{ij}	183.49	cm^{-1}
K_{ij}	140.54	cm^{-1}
ω_k	5.00	cm^{-1}
B_{ij}	0.0015	cm^{-1}

Table 3. Experimental data [26] and theoretically obtained values of dielectric constant for AFeSD crystal

Temperature (K)	Dielectric constant experimental	Theoretical calculation of dielectric constant
85	15.234	15.155
86	18.708	19.884
87	29.242	30.786
88	74.531	74.462
89	63.864	63.444
90	57.964	56.636
91	53.458	51.829
92	50.141	48.121
93	45.846	44.295
94	41.012	40.348
95	39.364	38.199
96	38.436	37.052
98	36.894	35.615
100	34.647	33.466
102	32.756	31.674
104	30.022	29.526

Table 4. Experimental data [26] and theoretically obtained values of loss tangent for AFeSD crystal

Temperature (K)	Loss tangent experimental	Theoretical calculation of loss tangent
85	0.304	0.307
86	0.328	0.317
87	0.422	0.369
88	0.941	0.938
89	0.849	0.854
90	0.819	0.802
91	0.773	0.758
92	0.743	0.725
93	0.708	0.688
94	0.665	0.656
95	0.632	0.641
96	0.619	0.629
98	0.602	0.614
100	0.595	0.607
102	0.586	0.599
104	0.581	0.586

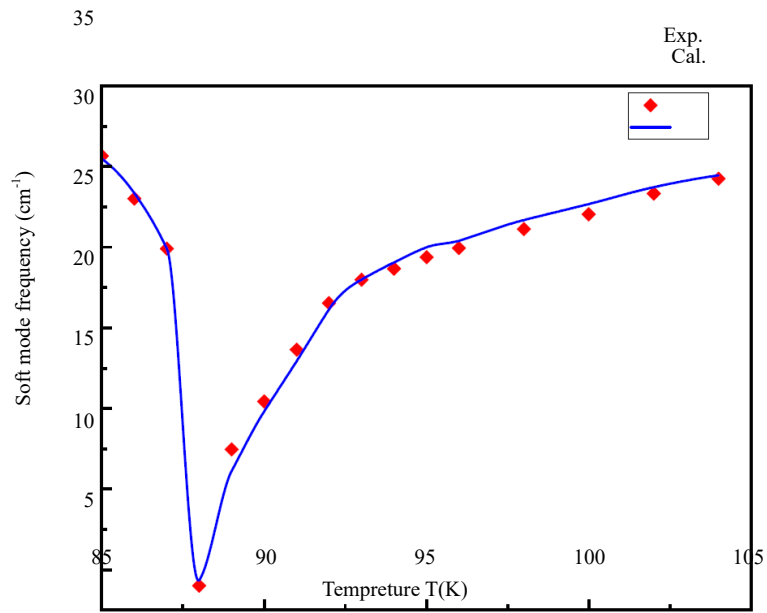


Figure 2. Thermal variation of soft mode frequency for AFeSD-alum (symbols: correlated values with experimental data [26]; solid line: present theory)

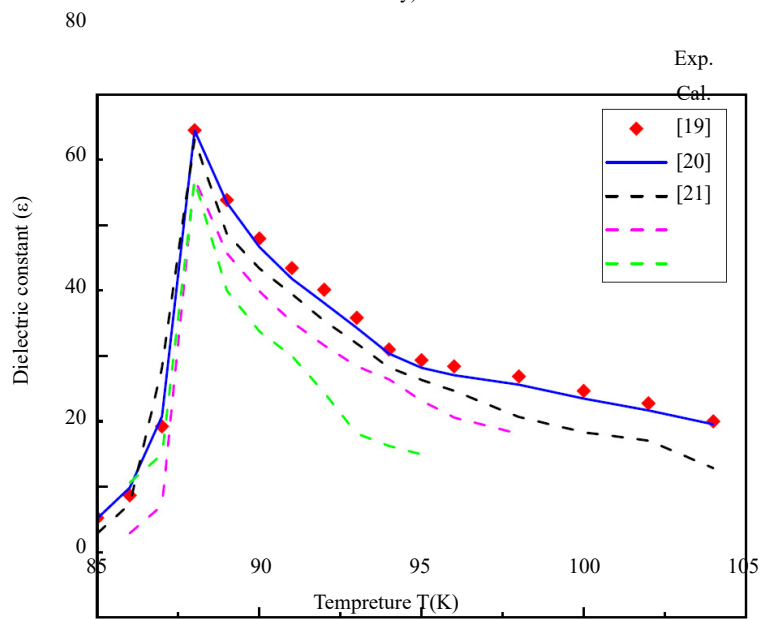


Figure 3. Thermal variation of dielectric constant for AFeSD-alum (red diamond: experimental data)

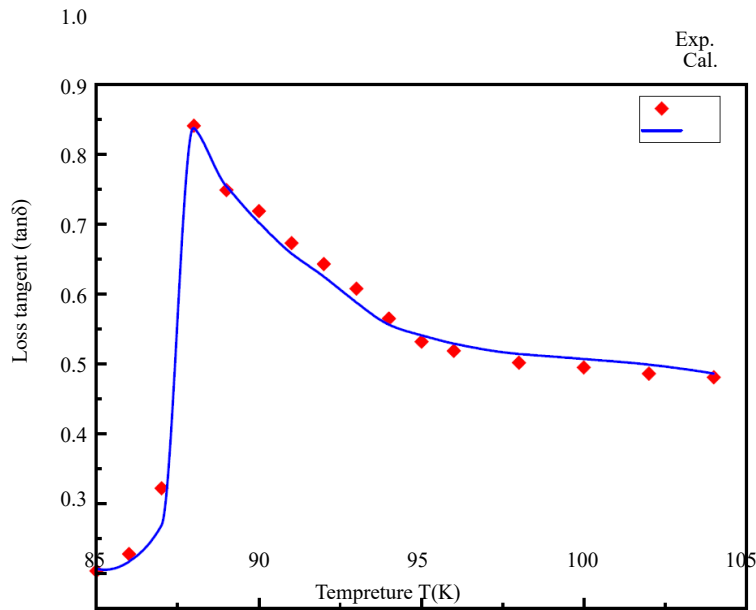


Figure 4. Thermal variation of loss tangent for AFeSD-alum (symbols: correlated values with experimental data [26], solid line: present theory)

8. Results and Discussion for AFeSD-alum

In the present paper, by modifying the extended two sublattice pseudospin lattice coupled-mode model, Hamiltonian has used to explain the dielectric properties of AFeSD-alum. We have added the anharmonic phonon interactions, indirect spin-lattice couplings, and direct spin-spin coupling together with an external electric field in the modified model Hamiltonian. With the help of Green function theory and modified two sublattice model Hamiltonian, we have derived the expressions for energy shift, line width, ferroelectric mode frequency, dielectric permittivity, and dielectric loss tangent properties. By setting the model values of various physical parameters given in table (1) and by using the equations (32), (35), and (36), the temperature variations of the ferroelectric mode frequency ($\widehat{\Omega}$), dielectric permittivity $\varepsilon(\omega)$ and dielectric loss tangent $\tan \delta$ have been obtained and depicted in figures (2), (3), and (4). The obtained results for ferroelectric soft mode frequency dielectric constant permittivity, and tangent loss depicted in figures (2), (3), and (4), respectively, and compared well with experimental results reported by others [26] for dielectric constant, loss tangent, and correlated data for ferroelectric mode frequency for AFeSD-alum compound. Our theoretical results agree well with the experimental results reported by Mitsui [26].

Therefore, from figure (2) and equation (32), it is observed that the ferroelectric mode frequency ($\widehat{\Omega}$) decreases as we approach the low-temperature side towards the phase transition temperature. At Curie temperature (T_c) ferroelectric frequency becomes infinitesimally small and then increases above it as the value of temperature increases. Our obtained result for ($\widehat{\Omega}$) is in good agreement with experimental observations. From figure (3) and equation (35), relative permittivity initially increases as the value of temperature increases from the low side and becomes anomalously large at Curie temperature (T_c). Above the Curie temperature, the dielectric permittivity value decreases with the increasing value of temperature. Our obtained result for dielectric constant is in good agreement with experimental observations of Mitsui [26] and the similar behaviour obtained for loss tangent ($\tan \delta$) and equation (36) for AFeSD-alum crystal depicted in figure (4).

9. Conclusions

In the present study, from the above results and discussion, we can be understood well that with the help of retarded Green function theory along with the two-sublattice pseudospin lattice coupled-mode model Hamiltonian extended with anharmonic phonon couplings, indirect spin-lattice couplings, direct spin-spin coupling together with an external electric field explains the phase transition properties of AFeSD-alum crystal clearly. The 3rd- and 4th-order phonon anharmonic interaction terms significantly affect the thermal variations of soft mode frequency, dielectric permittivity, and dielectric tangent loss properties in ferroelectric AFeSD-alum crystal. As the earlier authors [19–21] used a simple decoupling method and decoupled the correlations at initial steps, due to which some critical interaction results disappeared from their results. The energy shift and line width are contained in the additional terms of the present work. This ultimately provides the renormalized ferroelectric soft mode frequency. Our theoretical obtained results are better than earlier authors' results [19–21], quantitatively. Unlike the case of hydrogen-bonded ferroelectrics, very little or no isotope effect is observed on the transition temperatures indicating that the H bonds are not primarily involved in the transition mechanisms of alums having a large number of H bonds. The dielectric constant in AFeSD alum follows the Curie-Weiss law in different temperature ranges with only one Curie-Weiss constant (C). Similar behaviour found in loss tangent. The soft modes in ferroelectric crystals are the typical polar modes. A soft mode is not always a polar mode but for ferroelectric transitions it is always a polar mode. Above Curie temperature (T_c), the soft mode is the lowest frequency transverse optic phonon (TO). Below T_c , the soft mode becomes a symmetric mode. Therefore, it is Raman active. In typical cases, its frequency follows the equation $\omega_{TO}^2(k=0) = a|T - T_c|$, where a is a constant [23]. Raman spectra of soft modes in the ferroelectric phase ($T < T_c$) depends on the angle between the spontaneous polarization and the phonon propagation direction. Soft mode frequencies for $k = 0$ modes are related to the dielectric constant by Lyddane-Sachs-Teller relation [24] defined as, $\frac{\epsilon_0}{\epsilon_\infty} = \frac{\omega_{LO}^2}{\omega_{TO}^2}$, where ϵ_0 is the static dielectric constant and ϵ_∞ is the high-frequency limit of the dielectric function. For soft mode $\omega_{TO} \rightarrow 0$ we see that $\epsilon_0 \rightarrow \infty$, a characteristic of ferroelectricity. This relation produces one essential anomaly needed to explain a ferroelectric transition. This relation produces one essential anomaly needed to explain a ferroelectric transition. Authors concluded that our calculations predict dielectric constant which can be potential applications in ferroelectric materials such as memory devices, capacitors, transducers, nonlinear optics, etc.

Acknowledgments

The authors are grateful to Prof. S.C. Bhatt (Ex-Convener and Head), Prof. P.D. Semalty (Ex. HOD Physics), Dr. Manish Uniyal, Dr. Shubhra Kala and Dr. Alok Sagar Gautam for their valuable suggestions; Department of Physics HNB Garhwal University and Department of Physics, Baba Ghulam Shah Badshah University for providing facilities and support in the work.

Conflict of interest

There is no conflict of interest for this study.

References

- [1] Jona, F.; Shirane, G. *Ferroelectric Crystals*; Macmillan: New York, NY, USA, 1962.
- [2] Wyckoff, R.W.G. *Crystal Structures*; John Wiley & Sons: New York, NY, USA, 1965; Volume 3.
- [3] Campbell, L.; De Benedetti, S. The Mössbauer effect hyperfine structure of a dilute ferric alum, $\text{NH}_4(\text{Al}, \text{Fe})(\text{SO}_4)_2 \cdot 12\text{H}_2\text{O}$. *Phys. Lett.* **1966**, *20*, 102–103.
- [4] Morup, S.; Thrane, N. Mössbauer Study of Electronic Spin-Flip Processes in $\text{NH}_4\text{Fe}(\text{SO}_4)_2 \cdot 12\text{H}_2\text{O}$. *Phys. Rev. B* **1971**, *4*, 2087.
- [5] Weber, H.J. Electrogyration effect in the paraelectric phase of ferroelectric alums. *Z. Krist. Cryst. Mater.* **1979**, *149*, 269–277.
- [6] Kopcewicz, M.; Kotlicki, A.; Szefer, M. Mössbauer study of proton irradiation effects in hydrated iron (II)

ammonium sulphate and iron (III) ammonium alum. *Phys. Stat. Sol. A* **1975**, *29*, 635–643.

- [7] Roberts, J.M.; Sambles, J.R. A study of spin relaxation phenomena in ammonium ferric alum $\text{NH}_4\text{Fe}(\text{SO}_4)_2 \cdot 12\text{H}_2\text{O}$ using Mössbauer spectroscopy and electron paramagnetic resonance. *J. Phys. Chem. Sol.* **1984**, *45*, 937–947.
- [8] Lou, S.H.; Yu, J.T. Dimorphism in methylammonium aluminum alum studied by X-ray diffraction and electron paramagnetic resonance. *Sol. Stat. Commun.* **1992**, *84*, 775–779.
- [9] Cha, Y.H.; Strauss, H.L. Local Structure and Tunneling Kinetics of Ammonium Aluminum Alum by Infrared Hole-Burning. *Straus. Inorg. Chem.* **2001**, *40*, 1176–1182.
- [10] Liu, S.; et al. *J. Chem. Ind. Eng. China* **2022**, *53*, 738–741.
- [11] Ilhan, F.; et al. *J. Hazard. Eng. China* **2008**, *154*, 381–389.
- [12] Mbow, M.L.; De Gregori, E.; Ulmer, J.B. Alum's adjuvant action: grease is the word. *Nat. Med.* **2011**, *17*, 415–416.
- [13] Gu, H.; Tian, P.; Li, Y.; Hao, X. Low-temperature electrolytic coloration and spectral property of ammonium alum crystals. *J. Lumin.* **2012**, *132*, 1623–1626.
- [14] Yauri, A.U.B.; Aliyu, M. Synthesis and Analysis of Potassium Aluminium Sulphate (Alum) from Waste Aluminium Can. *Int. J. Adv. Res. Chem. Sci.* **2014**, *1*, 1–6.
- [15] Gu, H.; Li, Y. Electrolytic coloration below 100 °C and spectral properties of potassium alum crystals. *Spectrochim. Acta Part A Mol. Biomol. Spectrosc.* **2015**, *139*, 342–345.
- [16] Gu, H.; Hao, X. Electrolytic coloration below 0 °C and spectral properties of ammonium alum crystals using a pointed anode. *Acta Part A Mol. Biomol. Spectrosc.* **2015**, *146*, 273–276.
- [17] Petrusovski, V.M. Vibrational spectra of hexaaquacomplexes. XII. On the possible anion disorder in selenate alums: prediction of the crystal structure and vibrational spectra of $\text{KAl}(\text{SeO}_4)_2 \cdot 12\text{H}_2\text{O}$ and related alums. *Maced. J. Chem. Chem. Eng.* **2015**, *34*, 73–85.
- [18] Abdeen, A.M.; et al. X-Ray and neutron diffraction study of alums. *Z. Krist. Cryst. Mater.* 1981, *157*, 147–166.
- [19] Chaudhury, K.R.; et al. Phenomenological explanation of the anomalous dielectric behavior of alums with pseudo-spin-lattice coupled-mode model. *Phys. Rev. B* **1982**, *26*, 6276.
- [20] Rawat, A.K.; Upadhyay, T.C.; Rawat, A. Temperature dependence of soft mode frequency and loss tangent of ammonium iron alum. *Indian J. Pure Appl. Phys.* **2017**, *55*, 683–686.
- [21] Mamgain, A.; Upadhyay, T.C. *Appl. Innov. Res.* **2020**, *2*, 86–92.
- [22] Svare, I.; Holt, R.M. Dielectric and proton relaxation from ammonium ion motion in alum. *Sol. State Commun.* **1979**, *29*, 851–853.
- [23] Petzelt, J.; Kozlov, G.V.; Volkov, A.A. Dielectric spectroscopy of paraelectric soft modes. *Ferroelectrics* **1987**, *73*, 101–123.
- [24] Blinc, R.; Zeks, B. Dynamics of order-disorder-type ferroelectrics and anti-ferroelectrics. *Adv. Phys.* **1972**, *21*, 693–757.
- [25] Zubarev, D.N. DOUBLE-TIME GREEN FUNCTIONS IN STATISTICAL PHYSICS. *Sov. Phys. Usp.* **1960**, *3*, 320.
- [26] Mitsui, T. *An Introduction to the Physics of Ferroelectrics*; Gordon and Breach: New York, NY, USA, 1976.
- [27] Cowley, R.A. The lattice dynamics of an anharmonic crystal. *Adv. Phys.* **1963**, *12*, 421–480.
- [28] Cochran, W. Crystal Stability and the Theory of Ferroelectricity. *J. Phys. Rev. Lett.* **1959**, *3*, 412.
- [29] Kubo, R. Statistical-Mechanical Theory of Irreversible Processes. I. General Theory and Simple Applications to Magnetic and Conduction Problems. *J. Phys. Soc. Jpn.* **1957**, *12*, 570–586.